Ionics, Volume 29, Issue 9, September 2023, pp. 3619-3627
DOI:10.1007/s11581-023-05096-7

Spatial Reticulate Polytriphenylamine Cathode Material with Enhanced Capacity for Rechargeable Aluminum Ion Batteries

Fei Tao[1], Guokang Wei[1,2,3] Xinqi Xu[1], Weize Xu[1], Wei Xie[4], Jianhong Yang[1], Zhenhua Luo[3], Xin Li[1], Jia Qiao[1,*]

[1] School of Materials Science and Engineering, Jiangsu University, 212013, Zhenjiang, China
[2] Cranfield Tech Futures Graduate Institute, Jiangsu University, 212013, Zhenjiang, China
[3] School of Water, Energy and Environment, Cranfield University, MK43 0AL, Cranfield, UK
[4] School of Food and Biological Engineering, Hezhou University, 542899, Hezhou, China
john_39842@163.com

Abstract. Rechargeable aluminum ion batteries (RAIBs) are a very attractive option for large-scale energy storage thanks to its promising theoretical capacity, high energy density, low cost, abundant earth resources, and environmental friendliness. While the cathode materials chosen and prepared are so essential for the electrochemical performance of RAIBs that extensive efforts and research have been done. In this study, the electrochemical performances of RAIBs were optimally improved by chemical polymerisation of triphenylamine to obtain polytriphenylamine (PTPAn) as the cathode material. The polymerisation process improved the spatial reticulate structure of triphenylamine, gained a three-dimensional mesh-like nano structure, which provided more chemical reaction sites and ion reaction channels, greatly increased the specific surface area, and accelerated the electrochemical reaction kinetics. On this basis, a stable discharge specific capacity around 137.4 mAh g^{-1} was achieved at high current densities of 1 A g^{-1} for the PTPAn cathode, and the Coulombic efficiency was maintained at about 99% after the life of 500 cycles. The understanding and appreciation of the charging and discharging working principle of PTPAn material as RAIBs cathode, meantime, were deepened by a multitude of *ex-situ* experiments. These findings are anticipated to serve as the cornerstone for the subsequent development of large-scale RAIBs systems for energy storage that use organic polymers as the cathode material.

Keywords: Rechargeable aluminum ion batteries; Organic cathode; Triphenylamine; Polytriphenylamine

1 Introduction

The growing demand for sustainable and environmentally responsible energy solutions has driven significant efforts in recent years to develop innovative energy storage technologies [1, 2]. In large-scale electrochemical energy storage devices, rechargeable batteries are essential components [3]. Thereinto, aluminum, being the third most abundant

element on earth and the least reactive metal, is easily extracted [4]. The aluminium ions (Al^{3+}) have a high theoretical volumetric capacity of 8046 mAh cm^{-3} and a corresponding high specific gravity capacity of 2980 mAh g^{-1}, and they have the ability to distribute three free electrons in an electrochemical process [5]. This has sparked extensive research into the development of Rechargeable Aluminum Ion Batteries (RAIBs) [6].

From the current state of research, RAIBs are still in their infancy and the main obstacle to their large-scale commercial application involves the new generation of active charge storage materials for cathodes [5, 7, 8]. Early studies favoured the high initial specific capacity of VI A transition metal compounds due to valence migration, but the subsequent cycle life and rate performance proved challenging to obtain because to the high Al^{3+} diffusion potential barrier and low electrical conductivity [9-11]. In contrast, the carbon-based materials have significant promise for strong rate performance and excellent cycle life due to their open-layer crystal structure and outstanding electrical conductivity [10, 12]. Applications especially to further improve the discharge specific capacity are still difficult to implement, however, due to the extensive issue of self-discharge, as well as the more difficult preparation procedures and higher application costs of some carbon materials [13].

Recent organic polyaniline RAIBs exhibit good specific capacity and a stable cycle life, which may indicate that the long-range benzene ring and quinone ring structures are stable as well as the activity of N functional groups as reaction sites, reflecting the potential research space in the derivatives of aniline and their polymers [14-17]. Still, the investigation of the underlying reaction processes and the creation of REDOX chemistry with adequate reversible participation of Al carriers (Al^{3+}, $AlCl_4^-$, $AlCl_2^+$ and $AlCl^{2+}$) remain major challenges [18].

A large quantity of organic polymer materials play an important role in the battery electrode and electrolyte system [19-22]. Among them, triphenylamine and its derivatives are particularly outstanding. They have received a great deal of interest and study in the realm of electrochemical energy storage devices because of their superior charge transfer properties [23, 24]. The center N atom of triphenylamine has a high capacity for electron transfer, a low ionization energy, and is easily oxidized to produce positive cationic free radicals [25]. As the cathode for a Li-organic battery, Chen et al. employed a functional star-shaped triazine triphenylamine framework, presented a multistage discharge voltage plateau during the charge-discharge process and exhibited a stable specific capacity of ~123 mAh g^{-1} [26]. By using straightforward electro-spinning and in-situ polymerization techniques, Mo and his colleagues created CNF@PTPAn composite membranes that operate as free-standing cathodes for high-performance sodium ion batteries., exhibited a high reversible capacity of 105 mAh g^{-1} [27].The findings demonstrate that trichromatic amines have high energy density and reversible REDOX characteristics, making them a potential cathode material.

Inspired by the above related researches, we took triphenylamine as the basic research object and polymerizes the corresponding polymer by chemical oxidation method with ferric chloride as oxidant. The chemical structure of the polymer is confirmed by XRD, FT-IR and Raman. The electrochemical performance of triphenyl and

its amine polymer electrode and the battery as RAIBs cathode material were investigated.

2 Experimental section

2.1 Materials Synthesis

Polytriphenylamine (PTPAn) was prepared by chemical oxidation of triphenylamine (TPAn) monomer. The synthesis was carried out as follows: first, 0.05 mol of TPAn was dissolved in chloroform ($CHCl_3$) under magnetic stirring; then, 0.2 mol of $FeCl_3$ was slowly added to the above solution and the reaction was carried out at room temperature with magnetic stirring for 6 hours; subsequently, the mixed solution was poured into methanol, during which the PTPAn produced was precipitated from the methanol solution. Finally, after filtration and four methanolic washes, the product is dried under vacuum at 80°C for 24 hours to give a pale yellow PTPAn primary product. The primary product was again dissolved in chloroform, filtered to remove insoluble impurities and the filtrate was poured into a mixture of acetone and 5% ammonia to precipitate once more. After filtration, the corresponding product was dried under vacuum at 50°C for 12 hours to give the final product, a pale yellow PTPAn powder.

2.2 Structural Characterization

The microscopic morphology and microstructure of materials were studied using transmission electron microscopy (TEM, HT-7800, Japan) and field-emission scanning electron microscopy (SEM, Requlus-8100, Japan). An INC 250 from Japan Electronic was utilised to map the samples using Energy dispersive X-ray spectrometry (EDX). The functional groups contained in the materials were investigated using Raman and Fourier-transform infrared spectroscopy (FT-IR, Thermo Scientific Nicolet iS50, USA). Raman spectroscopy was carried out using a Horiba Lab RAM HR Eolution analyser from Japan. A D8 Advance powder X-ray diffraction (XRD) from Bruker, Germany, was used to examine the crystalline structure of the material and to determine the physical phase type. On a Micromeritics ASAP 2460 from the USA, Nitrogen adsorption and desorption isotherms were performed. The X-ray photoelectron spectroscopy (XPS, Thermo Scientific K-Alpha, USA) was used to examine the surface chemical composition and valent states of the elements.

2.3 Electrochemical measurements

A typical RAIB was constructed using pure aluminium foil for the anode and the counter electrode, a Waterman GF/D glass fibre film as a separator, as illustrated in Fig. 1. Conducive carbon and PTFE were mixed with TPAn and PTPAn, respectively, and then coated on the molybdenum sheet to act as the cathode electrode in a weight ratio of 8:1:1. There was a bulk loading of around 2 mg of active material for each functional electrode.

A multichannel NEWARE battery test system was used to charge and discharge the electrodes under test and record the relative data change over time. CV testing was carried out using a PARSTAT MC electrochemical workstation from Princeton Scientific Instruments, USA. The test voltages ranged from 0.1 to 2.1 V and the sweep rates were varied from 0.1 to 2 m V s^{-1}. The same workstation was used for the EIS tests and a circuit was fitted to the test data, which was collected in the range of 100 kHz to 0.1 Hz.

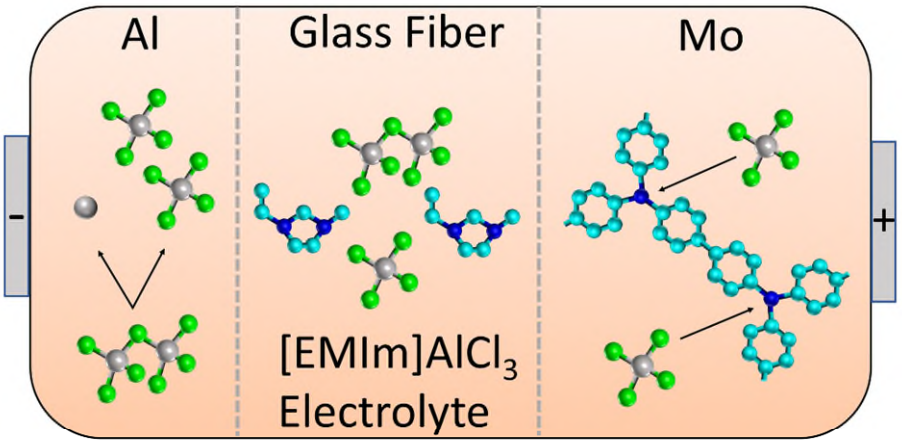

Fig. 1. The working principle in charging of RAIBs with PTPAn as cathode.

3 Results and discussion

3.1 Morphology and physiochemical properties

It can be seen from the SEM images in Fig. 2a and b that the monomers of TPAn have the structure of irregular blocks, while a few chains of PTPAn may firstly intertwine and stack to form a thicker main chain, and then demonstrate a distinct three-dimensional spatial mesh structure. Nanoparticles with a uniform distribution of about 50-100 nm were also grown on the chains, which may have been formed by the winding of long chains during the polymerization process. These are confirmed by the TEM image results in Fig.2d, e and f, TPAn monomers are sub-micron blocks with smooth surface diameter and 10-20 μm. While for PTPAn, the covering intertwining of chains is more obvious in some regions, and most of the chains disperse and form a better spatial reticulate structure. In Fig. 2c, some fine granular products can be observed on the PTPAn chain, which may be branched chains in the early stage of growth. The diameters of typical PTPAn chains are about 50-200 nm, and the diameter of the typical intermediate pores can be as high as 160 nm, and the larger could be up to 200-500 nm in diameter, facilitating the transmission of the doping anions and faster ion channels in chemical reactions.

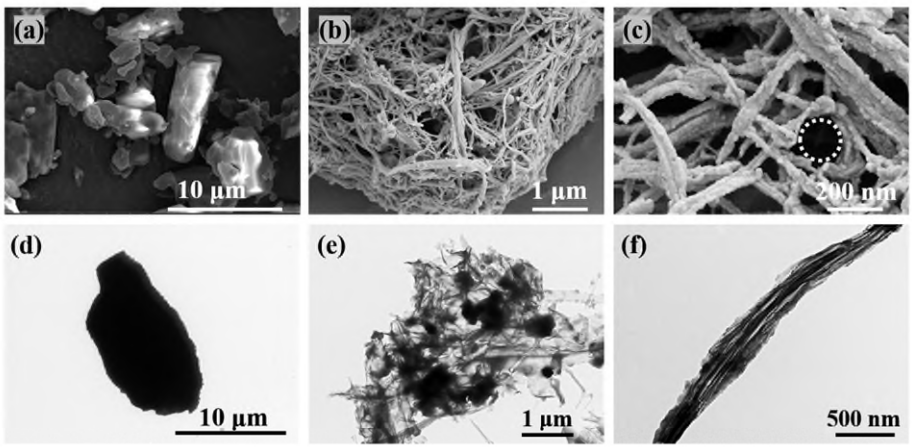

Fig. 2. SEM images of (a) TPAn and (b) PTPAn, SEM magnification images of (c) PTPAn, TEM images of (d) TPAn and (e) PTPAn, TEM magnification images of (f) PTPAn.

FT-IR spectrum in Fig. 3a displays a string of characteristic peaks at 1277, 1490, and 1592 cm^{-1}, which are indicative of the C-N bending, as well as the C-C and C=C ring stretching of TPAn, respectively. For the C-H bond, the out-of-plane wobble vibrations on the 1, 4-disubstituted benzene ring, and the bending vibrations on the benzene ring are represented by the peaks at the positions of 819, then 1177 and 1325 cm^{-1}. Importantly, PTPAn exhibits a novel peak at 819 cm^{-1} in the area corresponding to C-H out-of-plane vibrations, demonstrating that the structural unit of TPAn is connected by para-substituted benzene rings.

Additionally, Raman analysis was carried out to further determine the precise structure of TPAn and polymerized PTPAn by bonding modifications. Fig. 3b illustrates how the TPAn monomer significantly altered bond strength after polymerization. Stretching of the C=C ring at 1169 cm^{-1}, the C-N ring at 1287 cm^{-1}, and the C-H bending vibration at 1608 cm^{-1} all resulted in a considerable increase in peak strength of benzene ring, while the strength of the peaks at 999 and 1025 cm^{-1}, which stand for mono-substituted rings, dropped and dramatically eliminated at the same time, pointing to the formation of PTPAn.

The XRD patterns in Fig. 3c show a series of strong crystal diffraction peaks that are present in the TPAn monomer, together with the polymerized PTPAn, like other monomers subsequent polymerization, shows one single wide peak at $2\theta = 20°$, clearly displaying an amorphous structure[28]. In addition, PTPAn was found to have a large specific surface area of 44.63 m2 g^{-1} as opposed to a small one of TPAn with 0.05 m2 g^{-1} (Fig. 3d), resulting in its increased penetration in the electrolyte and the potential to greatly boost the electrochemical performance of the PTPAn cathode as RAIBs.

The effectively synthetization of PTPAn has been further demonstrated and confirmed by these outcomes after the proper aggregation procedure, and its high ratio

surface and excellent porosity make it a potential choice for the outstanding performance cathode material for RAIBs.

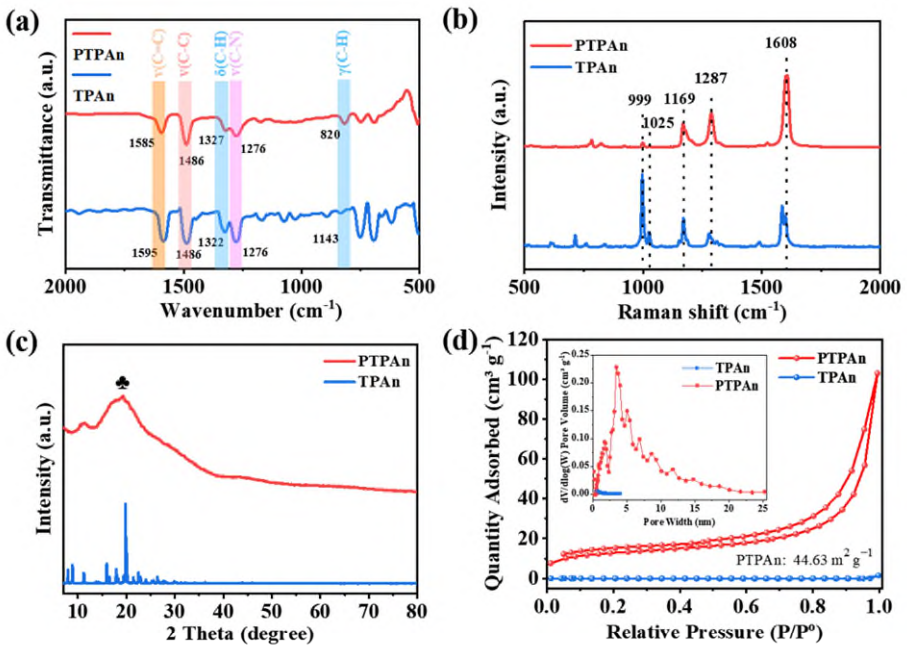

Fig. 3. TPAn and PTPAn figures of (a) FT-IR spectra, (b) Raman spectra, (c) XRD patterns and (d) N_2 sorption isotherms, the inset showed the pore size distribution.

3.2 Electrochemical performance

Two materials were prepared as the cathode for RAIBs and tested to find out their electrochemical performance. The cyclic performance of TPAn and PTPAn cathodes at a 1 A g^{-1} current density is shown in Fig. 4a. Whereas the PTPAn cathode has an initial discharge specific capacity of 81.3 mAh g^{-1}, the PTPAn cathode has a capacity of 34.9 mAh g^{-1}. Over the first 300 cycles, both of their specific capacities have a rising trend. The specific capacity of PTPAn and TPAn cathodes both increase in the initial 300 cycles while the raise of the former is significantly higher than that of the latter. After that, PTPAn stabilizes at 136-137 mAh g^{-1}, with Coulombic efficiency of 98-99%, while TPAn stabilizes at 41-42 mAh g^{-1}, with Coulombic efficiency of 93-94%, indicating that PTPAn has excellent charge-discharge performance. Moreover, additional charge-discharge tests were carried out on PTPAn cathodes with different mass loadings at the current density of 1 A g^{-1}. As shown in Fig. 3Sd, the specific discharge capacity of 2.5 mg cathode stabilizes at 88.1 mAh g^{-1} after 500 cycles. The specific

capacity of the 3.5 mg cathode is lower than 76.6 mAh g^{-1} after 300 cycles and shows a trend of continuous decline. These indicate that the higher load may reduce the actual conduction efficiency of ions and electrons for the cathode material, resulting in disappointing electrochemical performance. The charge-discharge curves of PTPAn in various cycles over a voltage range of 0.1-2.1 V at a current density of 1 A g^{-1} are shown in Fig. 4b. The PTPAn has a remarkable cycling performance, exhibiting initial discharge specific capacities of 81.3 mAh g^{-1}, and 112.5 mAh g^{-1} of 100th, 135.6 mAh g^{-1} of 300th, and 136.7 mAh g^{-1} of 500th, and the rising trend demonstrates a promising cycling performance.

Fig. 4c shows the rate performance of TPAn and PTPAn cathodes at different current densities. Compared to a current density of 0.2 A g^{-1}, the average capacity retention of PTPAn at a high current density of 1 A g^{-1} is 84.7%. Compared to 80.5% for TPAn, it is actually a very significant performance improvement when the former has a stable discharge specific capacity of over 3.3 times that of the latter. In addition, after being charged and discharged at a higher current of 2 A g^{-1}, with a capacity retention rate of around 100%, the PTPAn was capable of maintaining a discharge specific capacity of 124 mAh g^{-1} at a current density of 1 A g^{-1}, demonstrating the outstanding cycle stability, together with a good rate performance and reversibility. Fig. 4d shows the charge-discharge curves of PTPAn in the voltage range from 0.1 V to 2.1 V at different current densities. The discharge specific capacity of PTPAn was 143.8 mAh g^{-1} of 0.2 A g^{-1}, 141.2 mAh g^{-1} of 0.5 A g^{-1}, 124.1 mAh g^{-1} of 1 A g^{-1}, and 96.4 mAh g^{-1} of 2 A g^{-1}, verifying the good rate performance of PTPAn Cathode.

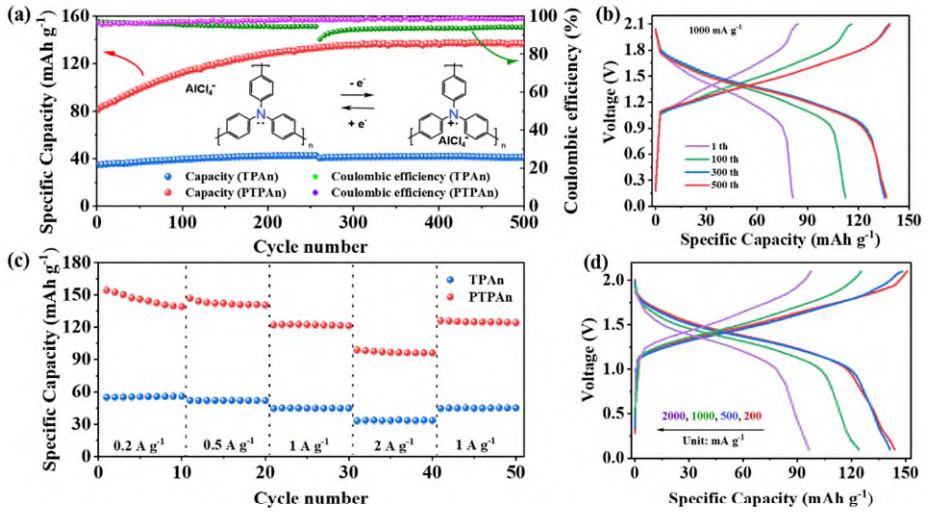

Fig. 4. (a) Cycling performance and the Coulombic efficiency of the TPAn and PTPAn cathode at a current density of 1 A g^{-1} with the cut-off voltage of 2.1 V, (b) Specific capacities of the PTPAn cathode after different cycles from 1st to 500th, (c) Specific capacities of the TPAn and PTPAn cathode at different current densities from 0.2 to 2 A g^{-1}, (d) Typical charge-discharge voltage profiles of the PTPAn at different current densities.

To evaluate the electrochemical performance of the prepared cathode materials, the electrochemical performance of TPAn and PTPAn was characterized by galvanostatic charge-discharge (GCD) and cyclic voltammetry (CV). Typical CV curves for TPAn and PTPAn electrodes were scanned over the potential range of 0.1-2.1 V (Fig. 5a and b). Notably, three pairs of REDOX peaks appear at 1.22 V, 1.46 and 1.74 V vs. Al/ Al^{3+} for TPAn charging, and at 1.66 V, 1.31 V and 1.06 V for discharging (vs. Al/Al^{3+}). Similarly, three pairs of REDOX peaks were found for PTPAn at 1.25 V, 1.52 and 1.81 V during charging and 1.67 V, 1.36 V and 1.09 V during discharging (vs. Al/Al^{3+}). In addition, the specific charge-discharge capacity of PTPAn was found to be much higher than that of TPAn cathode. In a typical charge-discharge curve, at a current density of 1 A g^{-1}, the specific charge and discharge capacities of TPAn were 45.0 and 42.5 mAh g^{-1}, respectively, with a Coulombic efficiency of 94.4%, whereas the specific capacities of PTPAn were 138.3 and 135.7 mAh g^{-1}, respectively, with a Coulombic efficiency of 98.1%. It can be seen that the discharge specific capacity and Coulombic efficiency of PTPAn are significantly better than those of TPAn, with an improvement rate of 219.3% and 3.9%, respectively. It is worth noting that the discharge platforms of the two cathode materials differ dramatically, PTPAn has a wider size, a longer range, and a more gradual fall tendency, whereas TPAn is the absolute reverse. A smaller polarization could be observed in PTPAn, indicating a more stable structure and then a better electrochemical performance compared to TPAn.

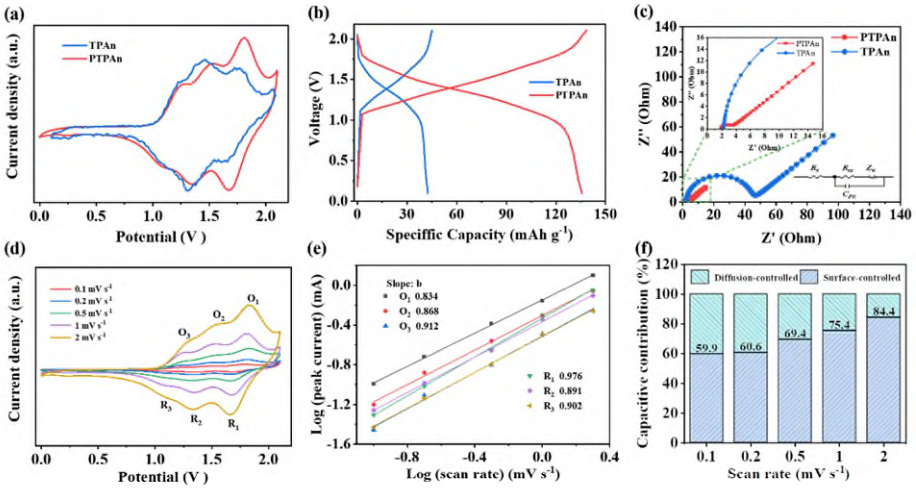

Fig. 5. (a) CV curves of TPAn and PTPAn cathodes at a scan rate of 1 mV s^{-1}, (b) Typical charge-discharge voltage profiles of the TPAn and PTPAn, (c) Nyquist plots of the TPAn and PTPAn cathodes, (d) CV curves of PTPAn cathode at various scan rates from 1 to 2 mV s^{-1}, (e) linear fitting of log(*i*) vs. log(*v*) for PTPAn, (f) contribution ratio of Pseudo-Capacitive of CV curves of PTPAn at various scan rates from 0.1 to 2 mV s^{-1}.

The improved electrochemical performance and Coulombic efficiency can be explained by the EIS measurements after 20 cycles at a current density of 1 A g^{-1}, determining the low ohm resistance and charge transfer resistance of PTPAn, as shown in Fig. 5c. The findings indicate that the polymerization has little impact on the samples of ohm resistance changes from 2.2 to 1.9 Ω, it has not changed by orders of magnitude or can even be barely described as essentially the same. On the contrary, it clearly reduces the charge transfer resistance from 47.3 to 3.5 Ω, and the smaller impedance is advantageous to the operation and utilization of RAIBs. In combination with the results of the morphology in Fig. 2c and the N_2 sorption isotherms in Fig. 3d, the fast ion transfer channels produced by the ideal spatial reticulate configuration of PTPAn, as well as the high specific surface area and numerous reaction sites produced by the widely dispersed nano-protrusions on the chain surface, not only accelerate the speed of chemical processes in the RAIBs and increases the contact surface between PTPAn and the electrolyte but also facilitate ion doping/de-doping and REDOX reactions.

A typical CV curve for the PTPAn cathode at different scan rates is shown in Fig 5d. Three pairs of REDOX peaks are evident in the curves and as the scan rate increases, the reduction peak shifts to lower potentials while the oxidation peak shifts to higher potentials. The electrode polarisation at the increased scan rate is to blame for this [29]. In Fig. 5e, the constant *b* for PTPAn of O1, O2, O3, and R1, R2, R3 are 0.834, 0.868, 0.912, 0.976, 0.891 and 0.902, respectively. This suggests that RAIBs facilitated more pseudocapacitive kinetics in the REDOX processes occur at high voltages. The behavior of the pseudo-captative process can be further understood by Fig. 5f and Fig. S1, the pseudo-capacitance contribution of the electrode was calculated for different scan rates from 0.1 mV s^{-1} to 2 mV s^{-1}, and the pseudo-capacitance contribution of the PTPAn increased gradually with increasing scan rate, from 59.9% to 84.4%, indicating that its excellent rate capacity may be mainly due to the contribution of pseudo-capacitance kinetics [30]. In addition, the ion diffusion rate was studied in Figs. S3a-c. It is worth noting that, as shown in Fig. S3c, the slope of oxidation peak for the cathode of PTPAn is significantly higher than that of the TPAn cathode, which strongly indicates that PTPAn compounds have more prominent reaction kinetics.

3.3 Energy storage mechanism

In order to verify the working principle of PTPAn cathode material, especially, the specific reaction sites of PTPAn skeleton, *ex-situ* FT-IR and Raman tests were performed on PTPAn cathodes in different states. Combined with the Raman diagram of Fig. 6a, it can be seen that before and after charging and discharging, the C-N bond located at 1287 cm^{-1} has an obvious stretching vibration change. Combined with the FT-IR data of Fig. 6b, it can be seen that before and after charging and discharging, the v (C-N) bond located at 1276 cm^{-1} has an obvious stretching vibration change, and the intensity ratio of C=C bond (1585 cm^{-1}) and C-C bond (1486 cm^{-1}) also changes accordingly. It can be inferred from the two spectra that in the charge-discharge reaction of PTPAn,

the doping/dedoping reaction occurs mainly at the N position located in the middle of the three benzene rings.

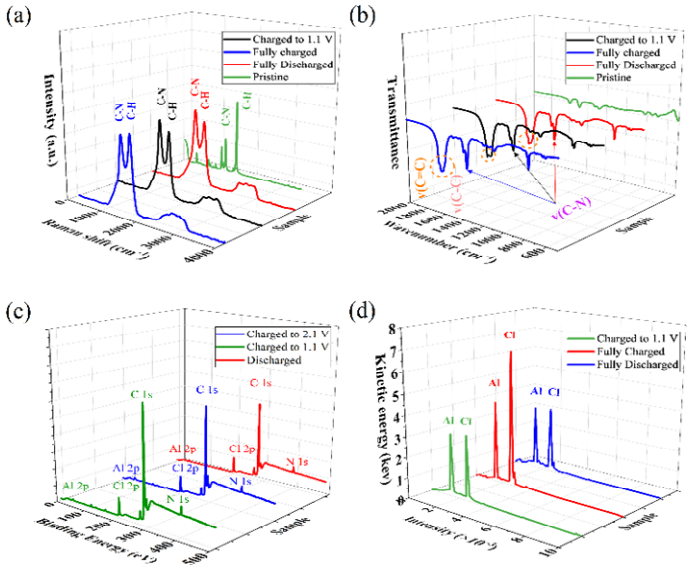

Fig. 6. Ex-situ data of (a) Raman spectra; (b) FT-IR spectra; (c) XPS spectra and (d) EDX spectra for PTPAn cathode at different state.

The EDX result would be supported by the *ex-situ* XPS results in Fig. 6c and S2, which reveal the outcomes with a considerable change of the Al and Cl elements in the sample completely charged to 2.1 V. Furthermore, EDX analysis and mapping on electrodes in various charge-discharge stages were carried out as shown in Fig. 6d that the kinetic energy of Al 2p and Cl 2p changed a lot during the charge-discharge process. More details could be found in the EDX mapping images of PTPAn. Electrical signals of the main skeleton of C and N elements were observed in the pristine sample (Fig. 7a). After charging to 1.1 V (Fig. 7b), a significant Al and Cl electrical signal is generated on the sample, which was different from the pristine sample indicating the doping of anions. A large number of Al and Cl signals are generated on a fully charged sample (Fig. 7c) and distributed fairly evenly throughout the electrode, while only a small number of Al and Cl signals are retained in a fully discharged sample (Fig. 7d). The traceable changes in the electrical signals of Al and Cl elements validate the doping/dedoping of anions during charge-discharge process, which further indicate the working principle of PTPAn cathode in RAIBs.

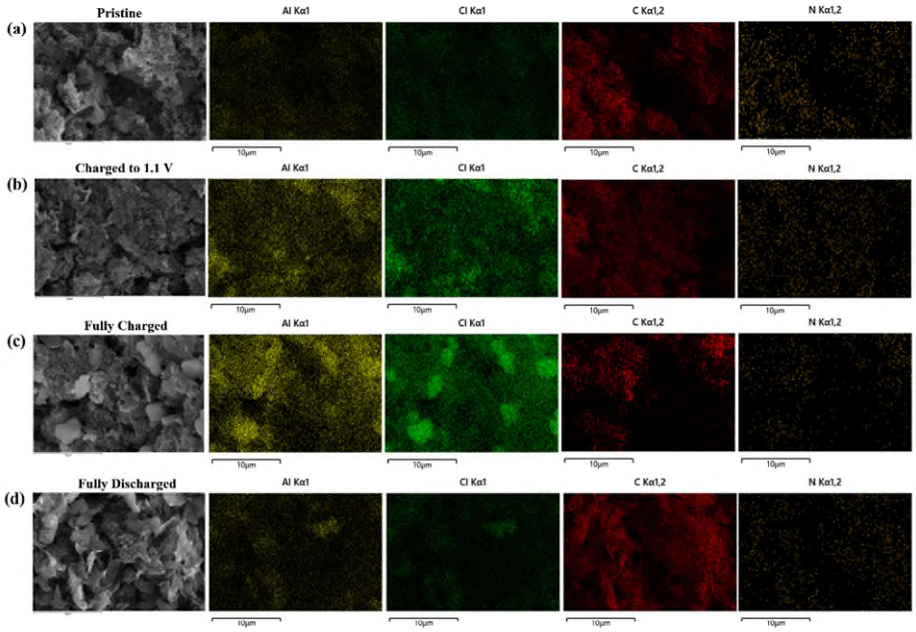

Fig. 7. EDX mapping images for Al, Cl, C and N of PTPAn in different states (a) Pristine; (b) Charged to 1.1 V; (c) Fully charged to 2.1 V and (d) Fully discharged to 0.1 V.

The working principle of PTPAn cathode in RAIBs could be then described as: At the cathode, $AlCl_4^-$ anions are dopes onto PTPAn and release electrons during charging, while during discharging the reverse is true, with $AlCl_4^-$ and PTPAn detaching and absorbing electrons. At the anode, $Al_2Cl_7^-$ interconverts with Al and $AlCl_4^-$ through a charging and discharging process. This also corresponds to the typical charging and discharging plateaus in Fig. 5b, respectively. The specific reaction equation for the electrodes is shown below.

Cathode reactions:

$$PTPAn + \mathrm{n}\, AlCl_4^- - \mathrm{n}\, e^- \leftrightarrow PTPAn(AlCl_4)_\mathrm{n} \quad (1)$$

Anode reaction:

$$4\mathrm{n}\, Al_2Cl_7^- + 3\mathrm{n}\, e^- \leftrightarrow \mathrm{n}\, Al + 7\mathrm{n}\, AlCl_4^- \quad (2)$$

4 Conclusion

In summary, we have developed a PTPAn material for RAIBs cathode by polymerizing TPAn monomers. The polymerisation process improves the spatial structure of the organic skeleton, allowing the TPAn to grow from a single particle into a three-dimensional spatial reticulate structure, greatly increasing the specific surface area of the material and providing a greater pseudo-capacitance contribution. This PTPAn cathode has a stable specific capacity around 137.4 mAh g^{-1} at 1 A g^{-1} (about 3.3 times higher compared to TPAn) with a Coulombic efficiency of around 99% and a life of 500 cycles. The retention rate of specific capacity is 84.5 % with good rate performance after the current density is expanded by 5 times (from 0.2 to 1 A g^{-1}). This indicates that the polymerisation significantly enhanced a better electrochemical performance of PTPAn than that of the TPAn monomer. The working principle of the PTPAn cathode material is also discussed through various *ex-situ* tests. These results lead to a better understanding of the organic conducting polymer PTPAn as the RAIBs cathode material and demonstrate its potential.

Acknowledgements

The authors thank the support from Institute of Green Materials and Metallurgy, School of Materials Science and Engineering and Cranfield Tech Futures Graduate Institute of Jiangsu University, Youth Fund project of Natural Science Foundation of Jiangsu Province, and School of Water, Energy and Environment of Cranfield University.

Funding

This work was supported by the Institute of Green Materials and Metallurgy, Jiangsu University (No. 4023000047, 4023000048), Youth Fund project of Natural Science Foundation of Jiangsu Province (No. BK20200898), Incubation Fund of School of Materials Science and Engineering, Jiangsu University, Scientific Research and Technology Development Project of Hezhou (No. HEKEJI20012).

Declarations

Authors' Contributions

FT did the investigation and prepared figures 1-9.
GW did the data curation and wrote the main manuscript text.
XX and WX (Weize Xu) did the formal analysis and resources parts.
WX (Wei Xie), ZL, JY, XL and JQ did the supervision, writing-reviewing and editing.
All authors reviewed the manuscript.
All authors have read and approved the manuscript.

Conflicts of Interest

The authors declare that they have no known competing financial interests or personal relationships that could have appeared to influence the work reported in this paper.

Ethical Approval

The authors declare that that this declaration is “not applicable”.

Data availability

Data will be made available on request.

References

1. Yang H, Li H, Li J, Sun Z, He K, Cheng HM, et al. The Rechargeable Aluminum Battery: Opportunities and Challenges. Angew Chem Int Ed Engl. 2019;58(35):11978-96.
2. Dunn B, Kamath H, Tarascon JM. Electrical energy storage for the grid: a battery of choices. Science. 2011;334(6058):928-35.
3. Chu S, Cui Y, Liu N. The path towards sustainable energy. Nature Materials. 2016;16(1):16.
4. Hu Y, Sun D, Luo B, Wang L. Recent progress and future trends of aluminum batteries. Energy Technology. 2019;7(1):86-106.
5. Elia GA, Marquardt K, Hoeppner K, Fantini S, Lin R, Knipping E, et al. An Overview and Future Perspectives of Aluminum Batteries. Adv Mater. 2016;28(35):7564-79.
6. Lin M-C, Gong M, Lu B, Wu Y, Wang D-Y, Guan M, et al. An ultrafast rechargeable aluminium-ion battery. Nature. 2015;520(7547):324-8.
7. Zhou Q, Zheng Y, Wang D, Lian Y, Ban C, Zhao J, et al. Cathode materials in non-aqueous aluminum-ion batteries: Progress and challenges. Ceramics International. 2020;46(17):26454-65.
8. Zhang K, Kirlikovali KO, Suh JM, Choi J-W, Jang HW, Varma RS, et al. Recent advances in rechargeable aluminum-ion batteries and considerations for their future progress. ACS Applied Energy Materials. 2020;3(7):6019-35.
9. Wang H, Bai Y, Chen S, Luo X, Wu C, Wu F, et al. Binder-Free V2O5 Cathode for Greener Rechargeable Aluminum Battery. Acs Appl Mater Interfaces. 2015;7(1):80-4.
10. Wang S, Jiao S, Wang J, Chen HS, Tian D, Lei H, et al. High-performance aluminum-ion battery with CuS@C microsphere composite cathode. Acs Nano. 2016;11(1):469-77.
11. Nacimiento F, Cabello M, Alcántara R, Pérez-Vicente C, Lavela P, Tirado JL. Exploring an aluminum ion battery based on molybdite as working electrode and ionic liquid as electrolyte. Journal of The Electrochemical Society. 2018;165(13):A2994-A9.

12. Qiao J, Zhou H, Liu Z, Wen H, Yang J. Defect-free soft carbon as cathode material for Al-ion batteries. Ionics. 2019;25(3):1235-42.
13. Qiao J, Zhou H, Liu Z, Wen H, Du J, Wei G, et al. Dense integration of graphene paper positive electrode materials for aluminum-ion battery. Ionics. 2020;26(1):245-54.
14. Meng P, Huang J, Yang Z, Wang F, Lv T, Zhang J, et al. A Low-Cost and Air-Stable Rechargeable Aluminum-Ion Battery. Advanced Materials. 2022;34(8):2106511.
15. Wang S, Huang S, Yao M, Zhang Y, Niu Z. Engineering Active Sites of Polyaniline for AlCl2 (+) Storage in an Aluminum-Ion Battery. Angew Chem Int Ed Engl. 2020;59(29):11800-7.
16. Wang D, Hu H, Liao Y, Kong D, Cai T, Gao X, et al. High-performance aluminum-polyaniline battery based on the interaction between aluminum ion and -NH groups. Science China Materials. 2020;64(2):318-28.
17. Liao Y, Wang D, Li X, Tian S, Hu H, Kong D, et al. High performance aluminum ion battery using polyaniline/ordered mesoporous carbon composite. Journal of Power Sources. 2020;477.
18. Meng J, Zhu L, Haruna AB, Ozoemena KI, Pang Q. Charge storage mechanisms of cathode materials in rechargeable aluminum batteries. Science China Chemistry. 2021;64(11):1888-907.
19. Zhang H, Huang L, Xu H, Zhang X, Chen Z, Gao C, et al. A polymer electrolyte with a thermally induced interfacial ion-blocking function enables safety-enhanced lithium metal batteries. eScience. 2022(002):002.
20. Mu P, Zhang H, Jiang H, Dong T, Zhang S, Wang C, et al. Bioinspired Antiaging Binder Additive Addressing the Challenge of Chemical Degradation of Electrolyte at Cathode/Electrolyte Interphase. Journal of the American Chemical Society. 2021(43):143.
21. Wang C, Ma Y, Du X, Zhang H, Xu G, Cui G. A polysulfide radical anions scavenging binder achieves long-life lithium–sulfur batteries. Battery Energy. 2022;1(3):20220010.
22. Jiang M, Mu P, Zhang H, Dong T, Tang B, Qiu H, et al. An Endotenon Sheath-Inspired Double-Network Binder Enables Superior Cycling Performance of Silicon Electrodes. Nano-Micro Letters. 2022.
23. Peng Z, Yi X, Liu Z, Shang J, Wang D. Triphenylamine-based metal–organic frameworks as cathode materials in lithium-ion batteries with coexistence of redox active sites, high working voltage, and high rate stability. ACS applied materials & interfaces. 2016;8(23):14578-85.
24. Yamamoto K, Suemasa D, Masuda K, Aita K, Endo T. Hyperbranched triphenylamine polymer for ultrafast battery cathode. ACS applied materials & interfaces. 2018;10(7):6346-53.
25. Lian X, Zhao Z, Cheng D. Recent progress on triphenylamine materials: synthesis, properties, and applications. Molecular Crystals and Liquid Crystals. 2017;648(1):223-35.
26. Chen Z, Su C, Zhu X, Xu R, Xu L, Zhang C. Micro-/Mesoporous conjugated polymer based on star-shaped triazine-functional triphenylamine framework as the performance-improved cathode of Li-organic battery. Journal of Polymer Science Part A: Polymer Chemistry. 2018;56(22):2574-83.

27. Mo L, Zhou G, Ge P, Miao Y-E, Liu T. Flexible polytriphenylamine-based cathodes with reinforced energy-storage capacity for high-performance sodium-ion batteries. Science China Materials. 2022;65(1):32-42.
28. Ni W, Cheng J, Li X, Gu G, Huang L, Guan Q, et al. Polymeric cathode materials of electroactive conducting poly (triphenylamine) with optimized structures for potential organic pseudo-capacitors with higher cut-off voltage and energy density. RSC Advances. 2015;5(12):9221-7.
29. Li X, Zhang Y, Xing W, Li L, Xue Q, Yan Z. Sandwich-like graphene/polypyrrole/layered double hydroxide nanowires for high-performance supercapacitors. Journal of Power Sources. 2016;331:67-75.
30. Pu X, Zhao D, Fu C, Chen Z, Cao S, Wang C, et al. Understanding and calibration of charge storage mechanism in cyclic voltammetry curves. Angewandte Chemie. 2021;133(39):21480-8.

Spatial reticulate polytriphenylamine cathode material with enhanced capacity for rechargeable aluminum ion batteries

Tao, Fei

2023-09-01

Tao F, Wei G, Xu X, et al., (2023) Spatial reticulate polytriphenylamine cathode material with enhanced capacity for rechargeable aluminum ion batteries. Ionics, Volume 29, Issue 9, September 2023, pp. 3619-3627

https://doi.org/10.1007/s11581-023-05096-7